J Mol Model (2016) 22: 225
DOI 10.1007/s00894-016-3091-0

ORIGINAL PAPER

Exploring 3D structure of human gonadotropin hormone receptor at antagonist state using homology modeling, molecular dynamic simulation, and cross-docking studies

Amirhossein Sakhteman[1,2] · **Minasadat Khoddami**[3] · **Manica Negahdaripour**[4,5] · **Arash Mehdizadeh**[4,5] · **Mohsen Tatar**[4,5] · **Younes Ghasemi**[4,5]

Received: 10 May 2016 / Accepted: 8 August 2016 / Published online: 25 August 2016

Abstract Human gonadotropin hormone receptor, a G-protein coupled receptor, is the target of many medications used in fertility disorders. Obtaining more structural information about the receptor could be useful in many studies related to drug design. In this study, the structure of human gonadotropin receptor was subjected to homology modeling studies and molecular dynamic simulation within a DPPC lipid bilayer for 100 ns. Several frames were thereafter extracted from simulation trajectories representing the receptor at different states. In order to find a proper model of the receptor at the antagonist state, all frames were subjected to cross-docking studies of some antagonists with known experimental values (Ki). Frame 194 revealed a reasonable correlation between docking calculated energy scores and experimental activity values ($|r| = 0.91$). The obtained correlation was validated by means of SSLR and showed the presence of no chance correlation for the obtained model. Different structural features reported for the receptor, such as two disulfide bridges and ionic lock between GLU90 and LYS 121 were also investigated in the final model.

Keywords Cross-docking simulation · G-protein coupled receptors · Human gonadotropin receptor · Molecular dynamic simulation

Introduction

Gonadotropin releasing hormone (GnRh) is a decapeptide produced from hypothalamus neurons in the perioptic area of the anterior and arcuate nucleus of the mediobasal section [1]. Binding of this hormone to GnRH receptors (GnRHR) can modulate human reproductive behavior through release of follicle stimulating hormone (FSH) and luteinizing hormone (LH) [2, 3].

GnRHRs are considered as members of the G-protein coupled receptors family, which are among transmembrane proteins with seven helix bundles [4]. GPCRs respond to the extracellular signals by activation of different pathways inside the cell [5]. For instance, in case of GnRHRs, the biological response is transferred via initiation of inositol phosphate cascade [6]. GnRH analogs have been widely used in the treatment of many diseases, including precocious puberty, leiomyoma, cancer, endometriosis, and other gynecological abnormalities [7, 8]. The two types of GnRH receptors found in mammals possess different pharmacological effects. Since GnRHR type 2 is absent in humans, its role is being played by GnRHR-1 [9, 10]. Based on previous research on the structures of agonists and antagonists for GnRHR, it can be concluded that a great demand to find more potent ligands for this target has emerged [11–13].

Due to the lack of a proper 3D structure for this receptor, most studies in this field were limited to ligand based drug

Electronic supplementary material The online version of this article (doi:10.1007/s00894-016-3091-0) contains supplementary material, which is available to authorized users.

✉ Amirhossein Sakhteman
asakhteman@sums.ac.ir

[1] Department of Medicinal Chemistry, School of Pharmacy, Shiraz University of Medical Sciences, Shiraz, Iran

[2] Medicinal Chemistry and Natural Products Research Center, Shiraz University of Medical Sciences, Shiraz, Iran

[3] Shahrekord University of Medical Sciences, Shahrekord, Iran

[4] Department of Biotechnology, School of Pharmacy, Shiraz University of Medical Sciences, Shiraz, Iran

[5] Pharmaceutical Sciences Research Center, Faculty of Pharmacy, Shiraz University of Medical Sciences, Shiraz, Iran

design (LBDD) [14]. A set of small GnRH antagonists was reported by Lanier et al. and their quantitative structure activity relationship (QSAR) was revealed by computational approaches [15]. In another study, QSAR investigation of 128 non-peptide antagonists was performed [16]. Obtaining 3D conformations of GnRHR at different agonist and antagonist states can be helpful for structure based drug design studies [17, 18]. For this purpose, in this study a model of the receptor was suggested using templates with known 3D structure. Homology modeling studies of GPCRs have been remarkably reported as a computational tool to predict the structure of these transmembrane proteins [19–21]. In the next step, molecular dynamics (MD) simulation studies were performed to yield different conformations of the receptor. The simulation was performed within a lipid bilayer to study the receptor in physiological conditions. There are some conserved motifs of GnRHR in primates, such as a disulfide bridge at the location of CYS14-CYS200, which is essential for trafficking the receptor trough plasma membrane. Moreover, it was seen that GLY90 and LYS121 mutation triggers ionic lock distraction, which disables receptor signaling [22]. Thus, some experimental based structural features of the receptor, such as disulfide and salt bridges were considered and studied during simulation. Finally, cross-docking studies of the extracted frames with some known structures with available experimental activity (Ki) were performed. The frame with the most correlation between experimental and computational data was proposed to be used in structure based drug design studies (SBDD) [14]. A further validation method based on sum of the sum of log rank (SSLR) has also revealed that the current modeling approach was not found by chance correlations.

Materials and methods

A 24 core computational server running on Linux Ubuntu 12.04.3 LTS was used during MD and docking simulation studies. Preparation and visualization of the structures was done using a corei7 laptop running on windows 8 operating system. Bash scripting was used to run different experiments of this study. All scripts are provided in Supplementary information.

Homology modeling

Sequence of human Gonadotropin releasing hormone receptor (GnRH, ID code p30968) was adopted from the UniProt database (http://www.uniprot.org) as FASTA format [23]. The sequence was submitted to the I-TASSER (Iterative Threading ASSEmbly Refinement, http://zhanglab.ccmb.med.umich.edu/I-TASSER) server to identify acquired templates based on threading approach from the protein data bank. A restraint file to assign disulfide contacts between the residues CYS114-CYS196 and CYS14-CYS200 was prepared. Other parameters of modeling were remained as default.

The values of C-score as implemented in the I-TASSER server were used to select the best PDB structure for molecular dynamics simulation [24]. The model with the highest C-score value was thereafter submitted to the Procheck server for calculation of Ramachandran plot [25].

To orient the model based on the correct topology inside lipid bilayer, multiple servers were engaged for prediction of transmembrane helices.

The methods comprised TOPCONS (http://topcons.cbr.su.se) [26], HMMTOP (http://www.enzim.hu/hmmtop) [27], DAS (http://www.enzim.hu/DAS/DAS.html) [28], SOSUI (http://harrier.nagahama-i-bio.ac.jp/sosui) [29], TMHMM (http://www.enzim.hu/hmmtop) [30], TMpred (http://www.ch.embnet.org/software/TMPRED_form.html) [31], predict protein (https://www.predictprotein.org) [32], PolyPhobius (http://phobius.sbc.su.se/poly.html) [33], APSSP (http://imtech.res.in/raghava/apssp) [34], and ExPASY (https://www.expasy.org) [23].

Molecular dynamics simulation

GROMOS96 53A6 force field, as implemented in Gromacs4.5.5, was extended in such a way to include Berger lipid parameters [35]. Rotation and orientation of the receptor within a 128 DPPC bilayer was done using editconf and VMD softwares, respectively [36]. Translation of the receptor inside lipid bilayer was done based on the data obtained from transmembrane prediction servers.

InflateGro method was applied as an algorithm to embed the protein in the bilayer membrane. This method works by expanding the whole system in such a way to remove extra lipid residues and accommodate the protein [37]. Afterward, the system was subjected to iterative runs of shrinking and minimization to provide the favorable area per lipid for DPPC systems (62.9-64.2 Å) [38].

GridMAT-MD_v2.0 perl script was used for the calculation of area per lipid density during all steps of shrinking and minimization [39]. In the next step, water and ions were added to the system. The solvation procedure was done in a way to prevent penetration of water molecules inside hydrophobic parts of the lipid membrane. For this purpose, van der Waals radius of carbon atom was set to 0.3 Å. In the ionization step, a total concentration of 0.15 M NaCl was added to simulate the system at physiological concentrations. Subsequently, the system was subjected to a minimization step using steepest decent followed by two runs of NVT and NPT. During both equilibration experiments, protein backbone was restrained. In the case of NVT v-scale, a modified Berendsen was used, while in NPT, the Nose-Hover algorithm was used as an accurate thermostat. The Parinello-Rahman barostat was used in

the case of NPT simulation. The main run of simulation was done in periodic boundary condition (PBC) using particle mesh Ewald (PME) long range electrostatics. In order to allow enough time for conformational changes inside the receptor, a 100 ns MD simulation was performed on the whole system. Heat map analysis of all residues was done based on Cα fluctuations during simulation [36].

Receptor sampling

TCL scripting as implemented in VMD was used for sampling different conformations of the receptor. Accordingly, 250 PDB structures were uniformly extracted from the output file of MD trajectories covering all simulation time. The resulted PDB files were converted to pdbqt by assigning Gasteiger partial charges using MGLTOOLs 1.5.6 [40].

Ligands preparation

A set of 34 small molecule ligands with known experimental antagonist activity against GnRHR were retrieved from the CHEMBL database as SMILES strings [41]. The structures were subsequently converted to 3D mol2 using open babel 2.3.2. Meanwhile, the corresponding values of Ki for the compounds were converted into PKi (-logki) and was saved as a separate text file. The addition of Gasteiger partial charges and merging non-polar hydrogen atoms were done in the case of all structures using MGLTOOLS 1.5.6 to yield 34 pdbqt files.

Binding site prediction

The sequence of GnRHR was subjected to RaptorX (http://raptorx.uchicago.edu) for prediction of binding site based on a fold recognition approach [42]. In another experiment, the resulted model of I-TASSER was submitted to the CASTp (http://sts.bioe.uic.edu/castp; computed atlas of surface topography of proteins) server with a probe radius set to 1.4 Å in order to predict the possible cavities in the receptor [43].

Docking simulation

Coordinates of Cα for LYS121 were considered as the center of the grid box based on the results of the previous experiments and literature review. Calculation of grid box size was according to the equation below:

$$\text{Size}\,(x, y, z) = 2^{*}\,\text{LAD} = 30\ \text{Å} \quad (1)$$

Where LAD denotes the largest atomic distance in all data set. In the next step, 250*34 = 8500 cross docking simulations were done using the Vina 1.1.2 software [44]. Exhaustiveness value in Vina was set to 100 to perform effective docking simulations for all structures. Finally, the lowest energy scores of Vina were extracted as a matrix keeping receptor frames in columns and ligand structures as rows. The resulted matrix of data is supported in Supplementary information.

Analysis of docking results was done by calculating Pearson correlation coefficient between each column and the vector of pKi values. The frame with the best correlation coefficient was entered to an in-house application implemented in .NET in order to calculate SSLR [45]. VMD and pose view applications were used for the visualization and prediction of binding mode, respectively [36, 46]. Pattern for the interaction of all compounds with receptor was obtained by protein ligand interaction profiler (PLIP) (https://projects.biotec.tu-dresden.de/plip-web/plip/)[47].

Results and discussion

The alignment file used in the modeling procedure is displayed in Fig. 1. As seen, seven templates based on ten different threading methods were used in the modeling of the receptor. The used templates were 4n6h_A (structure of human delta opioid 1.8 Å), 2RH1_A (human beta 2 adrenergic receptor 2.4 Å), 1GZM_A (bovine rhodopsin 2.65 Å), 4IAR_A (chimeric protein of 5-HT1BRIL in complex with ergotamine 2.7 Å), 4PHU_A (human GPR40 2.33 Å), 4DJH_A (human kappa opioid receptor 2.9 Å), and 4GRV_A (the crystal structure of neurotensin receptor NTS1 in complex with neurotensin 2.8 Å). The highest identity among the used templates was attributed to 4DJH_A, 4GRV_A, and 4IAR_A (23 %).

The results of five top I-TASSER models based on their C-score values are displayed in Table 1. Higher values of C-score represent a model with more confidence. As seen in Table 1, model 1 revealed the highest C-score value. Meanwhile, TM-score of model 1 is more than 0.5, indicating its correct topology to be selected for further validation studies. In order to verify that the obtained model is similar to native proteins, a Ramachandran plot was calculated using the Procheck server [25]. As seen in Fig. 2, more than 90 % of the residues were located in the most favored regions of the plot. This shows that the conformational characteristics of the modeled receptor are similar to the native proteins.

Since topology of membrane proteins inside the lipid bilayer is very important prior to simulation studies, TM regions of GnRHR were predicted by different methods. As seen in Table 2, all methods shows similar results to Uniprot data in terms of predicting TM domains of the receptor. The next important step was to predict the binding of the receptor wherein two different methods were used for this purpose. One approach was based on spatial probes to find regions with the capability of accommodating small molecules as implemented in CASTp server and the other was based on

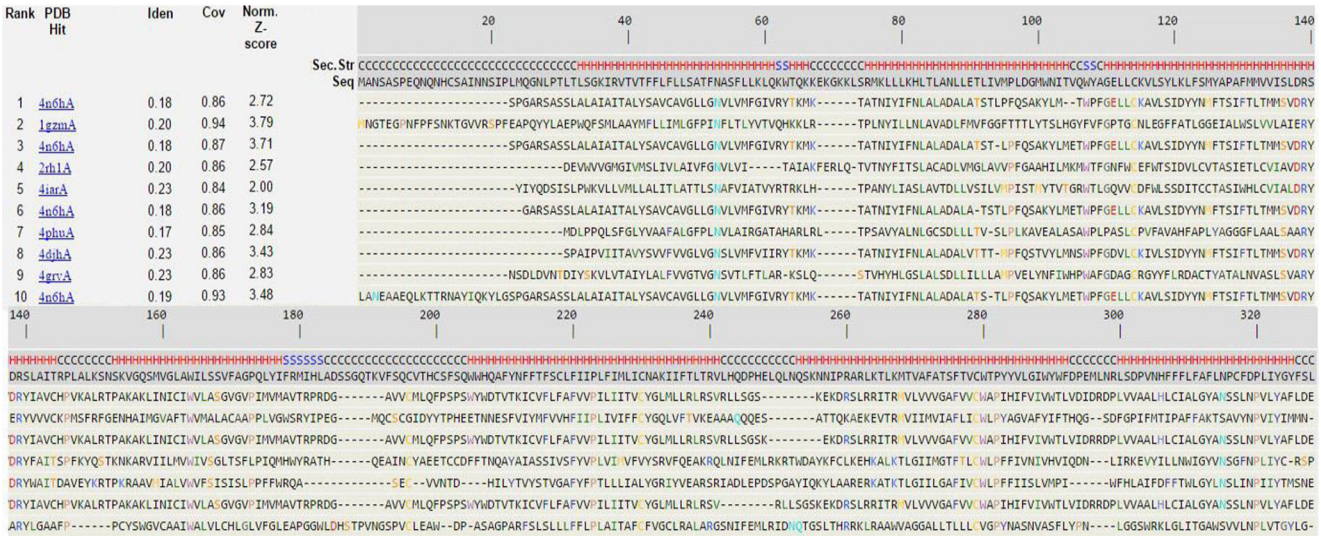

Fig. 1 Final alignment used for homology modeling of GnHR

conserved residues as implemented in RaptorX [43, 48]. The residues selected by Raptorx were ASP98, LUE117, LYS121, LEU122, MET125, CYS196, THR198, TYR211, ASN212, THR215, LEU219, TRP280, TYR283, TYR284, GLY287, ASN305, PHE309, and PHE313. Similar residues were also calculated based on CASTp server.

Being satisfied with the 3D model of the receptor and its topology, the next step was to perform molecular dynamic simulation in order to sample different conformations of the receptor in physiological conditions. A 100 ns MD simulation was performed on the whole system to reach an equilibrate state for the receptor based on RMSD variation of Cα and energy plot. As seen in Fig. 3, the system reached a steady state after 80 ns from the beginning of the simulation. Meanwhile the energy diagram of the system is showing that it is well equilibrated during simulation. In order to observe which parts of the receptor revealed more fluctuations during simulation, a heat map plot was calculated using the VMD software [36]. Figure 4 shows the fluctuation of Cα for each residue during MD. Based on the heat map study, the first extracellular domain of the receptor (1-21) showed a significant fluctuation after 10 ns from the beginning of the simulation. The residues 141-151, which are located in the cytoplasmic domain of the receptor have also revealed a large conformational change during simulation. The most significant fluctuation was however attributed to residues 181-191 in the second extracellular domain of the receptor. In order to obtain different conformations of the receptor for further docking studies, sampling of different frames were done based on 400 ps intervals. The obtained frames were subjected to cross docking simulation studies with known antagonists in order to investigate the frame with the most correlation toward experimental activity. Cα of the central residue LYS121 based on the two described methods (CASTp and RaptorX) and the literature was selected as the center of the grid box for docking studies. Pearson correlation of all docking frames with PKi values are depicted in Fig. 5. As seen, the most correlation

Table 1 C-score values of five top I-TASSER models

Model	C-score	TM-score
1	0.34	+0.76
2	−2.58	–
3	−2.20	–
4	−2.42	–
5	−2.58	–

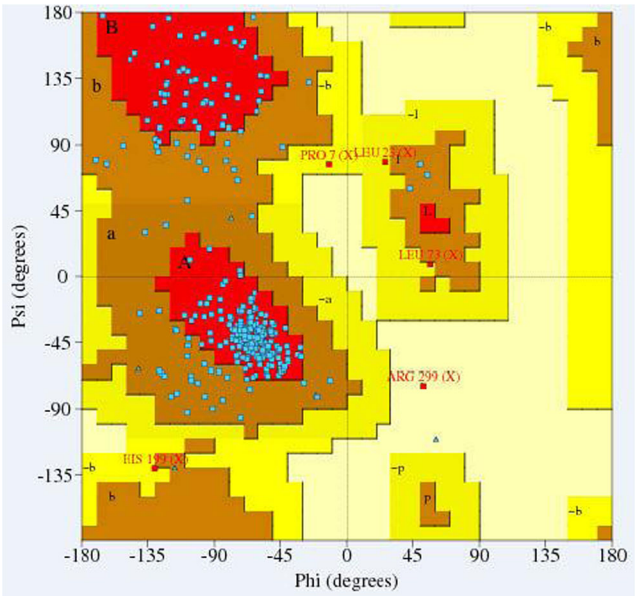

Fig. 2 Ramachandran plot of human GnRHR structure

Table 2 Transmembrane helices prediction of human gonadotropin releasing hormone receptor

Method	TM1	TM2	TM3	TM4	TM5	TM6	TM7
Uniprot	39 – 58	78 - 97	116 - 137	165 - 184	213 - 232	282 - 300	307 - 326
HMMTOP	39 – 58	83 - 101	116 - 135	160 - 178	209 – 229	269 – 288	307 - 326
TMHMM	39 – 58	79 - 101	116 - 138	159 - 181	209 - 231	270 - 292	307 - 326
TOPCONS	37 – 58	79 - 100	120 - 141	158 - 179	213 – 234	268 - 289	307 - 328
SOSUI	39 – 61	–	120 - 142	160 - 182	215 - 237	268 - 290	304 - 326
TMpred	37 – 58	82 - 106	116 - 137	155 - 178	209 - 232	268 - 286	303 - 326
DAS	37 – 54	83 - 95	117 - 137	162 - 171	213 - 236	277 – 286	307 - 326
Predictpr	39 – 61	78 - 99	118 - 139	156 - 176	211 - 233	269 - 291	303 - 326
Philius	37 – 58	78 - 100	122 - 141	158 - 178	211 - 232	268 - 288	306 - 326
SCAMPI	38 – 58	78 - 98	122 - 142	159 - 179	210 - 230	272 - 292	–
polyphobious	37 – 58	78 - 97	117 - 137	158 - 178	211 - 234	269 - 292	304 - 326

was observed in the case of frame 194 ($|r| = 0.91$). This result shows the most agreement between computational studies and experimental values for this frame. To ensure that this correlation was not obtained by chance, SSLR study was performed for the docking results of frame 194. SSLR is a non-parametric statistic method for evaluating the used scoring function in comparison with randomly ordered scores. Based on this method, the vector of random ranks is ordered by their inhibitory constants. Ordering of the scores was done in such a way that r_1 was the most active compound and r_n was the least active one. SSLR value was finally calculated according to the below equation (Eq. 2).

$$SSLR = n\log(r_1) + (n\text{-}1)\log(r_2) + \ldots + \log(r_n) \quad (2)$$

Where n is the number of compounds (n = 34). The obtained value of SSLR in this study was 691.60. This procedure was repeated for 1000 times with permuted values, and a p-value of 0.04 was calculated. It was therefore showing that a reasonable scoring function was used in this study. The final step was to obtain an overview for the binding mode of the structures in the cavity of GnRH receptor. For this purpose, the interaction maps of the receptor for all compounds were studied. The pattern for the interaction of all structures within the receptor are summarized in Table 3 and their corresponding pictures are provided in Supplementary information. Hydrophobic interaction with the residues TYR290 and TRP101, as reported in the literature, are seen for many structures of this study [10, 49]. Hydrophobic interaction with LEU117 and PHE308 were also seen in most structures. ASN212 was a key residue in hydrogen bonding interaction with many structures as in accordance with the literature [10, 49].

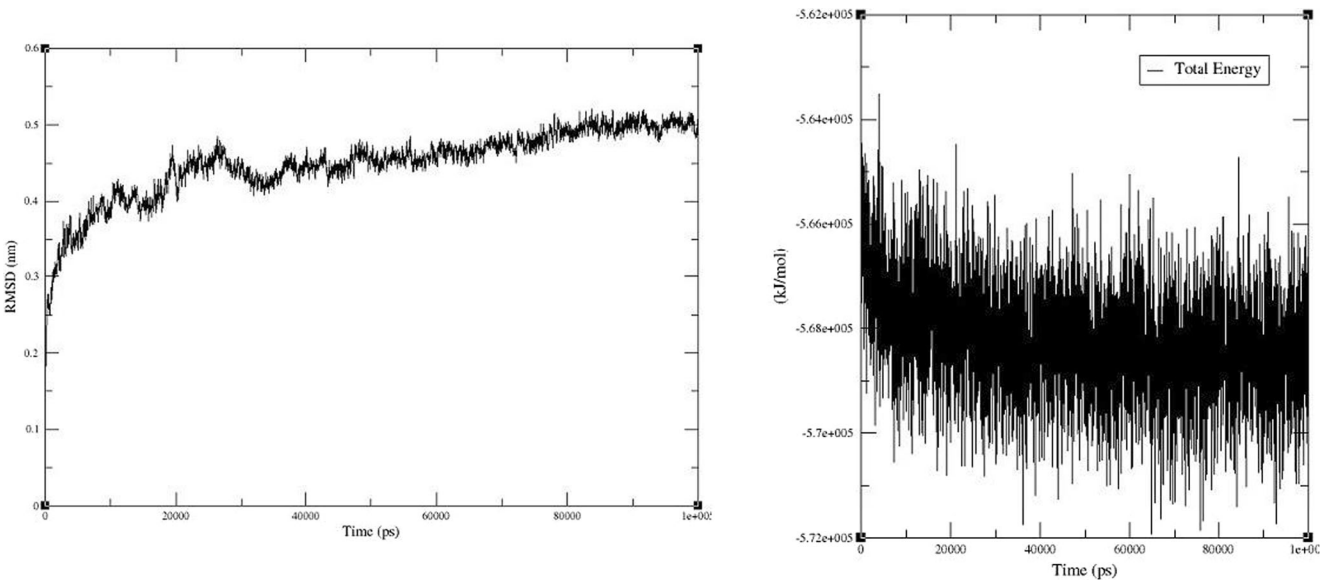

Fig. 3 RMSD of Cα during 100 ns MD simulation (left), energy plot of MD simulation (right)

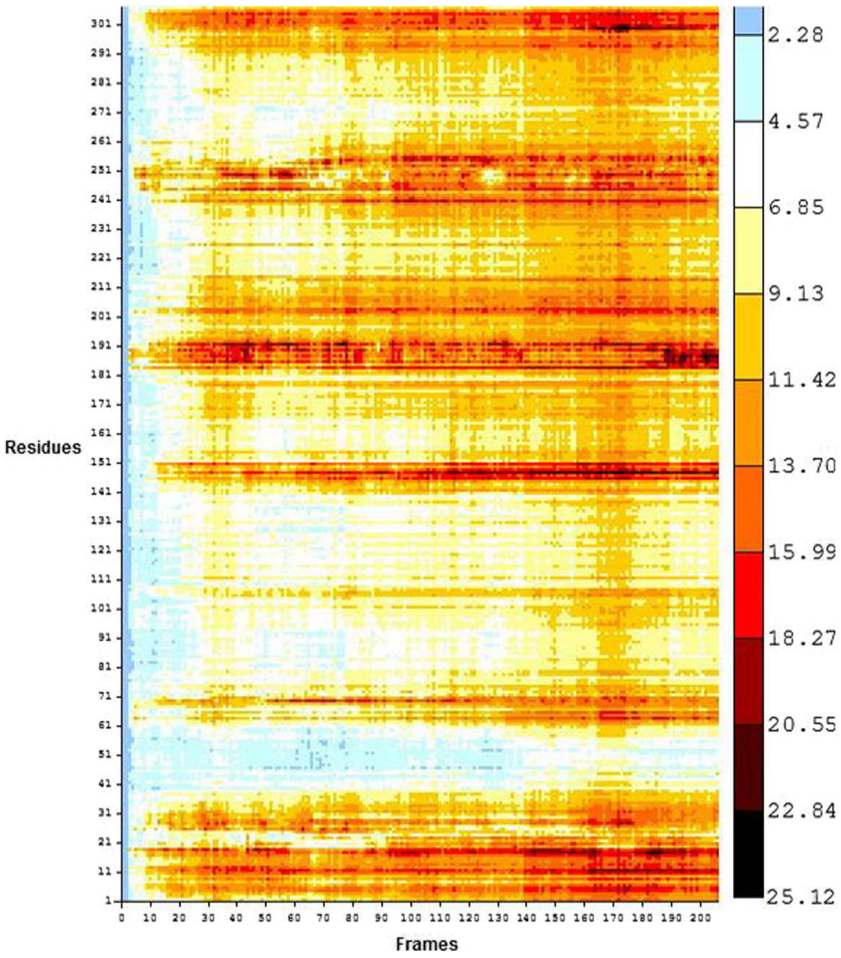

Fig. 4 Heat map analysis of protein backbone during 100 ns MD simulation

It was also found that TRP291, PHE308, TYR211, and HIS199 are the residues involved in π-π interaction with many ligands.

For instance, the binding site of the frame 194 with the most active compound, CHEMBL179691, is depicted in Fig. 6. CHEMBL179691 is a known antagonist (ki = 0.56 nM) and docking observation has also confirmed its suitable energy (-12.2 kcal mol^{-1}) [50]. It was seen that residues TYR291, LEU117, HIS199, and VAl304 were critical residues in the ligand receptor conjunction. In

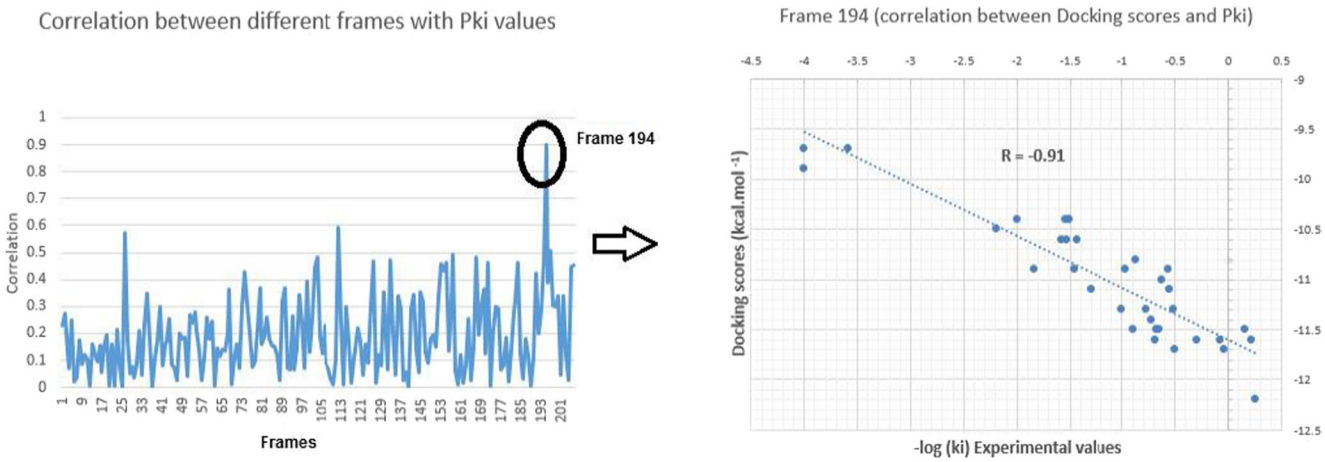

Fig. 5 Pearson correlation of all docking frames with experimental PKi values

Table 3 The structures used in the docking experiment together with their experimental and computational scores and interaction pattern with frame 194

CHEMBL ID	-log (ki)	Dock score (kcal mol^{-1})	Hydrophobic interactions	Hydrogen bonding	pi-pi stacking
CHEMBL179691	0.251	−12.2	TRP101, LEU117, LEU122, TYR211, THR215, TYR290, VAL304, PHE308, PHE308	CYS200, GLN208, ASN212, TYR283, TRP291	His199, TRP291
CHEMBL189164	−0.0414	−11.7	VAL94, TRP101, LEU117, LEU122, GLN174, TYR211, VAL304, PHE308	THR198, GLN208, ASN212, TYR283, TRP291	–
CHEMBL191817	−0.724	−11.4	VAL94, TRP101, LEU117, TYR211, TYR283, Val304, PHE308	TYR198, CYS200, GLN208, ASN212, TRP291	HIS199, PHE308
CHEMBL192172	−0.778	−11.3	VAL94, TRP101, LEU117, TYR211, TYR283, VAL304, PHE308	THR198, CYS200, GLN208, ASN212, TRP291	HIS199, PHE308
CHEMBL22653	−0.653	−11.5	TRP101, LEU117, LEU122, PHE170, TYR211, THR215, VAL304, PHE308	CYS200, ASN212, TYR283, TRP291	TRP291
CHEMBL255242	−1.832	−10.9	VAL94, TRP101, LEU117,TYR211, TYR283, VAL304, PHE308,	THR198, GLN208, ASN212, TRP291	–
CHEMBL257599	−1.301	−11.1	VAL94, LEU117, LYS121, TYR283, TYR290, VAL304, PHE308	SER118, GLN174, ASN212, TRP291	–
CHEMBL259906	0.217	−11.6	TRP101, LEU117, LYS121, GLN174, THR198, TYR211, TYR283, TYR290, VAL304, PHE308	ASN212, TRP291	–
CHEMBL359894	−0.505	−11.7	TRP101, TYR211, TYR283, VAL304, PHE308	THR198, CYS200, ASN212, TRP291	HIS199, PHE308
CHEMBL365985	−0.892	−11.5	TRP101, LEU117, LEU122, HIS199, TYR211, THR215, VAL304, PHE308	GLN208, ASN212, TYR283, TRP291	–
CHEMBL401632	−0.623	−11	VAL94, LEU117, LYS121, TYR283, TYR290, VAL304, PHE308	SER118, GLN174, GLN208, ASN212, TRP291	–
CHEMBL401807	−0.869	−10.8	LEU117, LYS121, TYR283, TYR290, VAL304, PHE308	SER118, GLN174, GLN208, ASN 212, TRP291	–
CHEMBL403234	0.155	−11.5	TRP101, LEU117, LEU122, GLN174, TYR211, TYR290, VAL304, PHE308	CYS200, GLN208, ASN212, TYR283, TRP291	TRP291
CHEMBL404180	−0.568	−10.9	TRP101, LEU117, LEU122, PHE170, TYR211, THR215, TYR290, VAL304, PHE308	CYS200, GLN208, ASN212, TYR283, TRP291	TYR283, TRP291
CHEMBL407719	−0.690	−11.6	VAL94, TRP101, LEU117, LEU122, PHE170, TYR211, THR215, TYR290, VAL304, PHE308	CYS200, GLN208,ASN212, TYR283, TRP291	HIS199, TRP291
CHEMBL444989	−1.518	−10.4	TRP101, LEU117, LEU122, PHE170, THR198, TYR211, THR215, TYR283, VAL304, PHE308	SER118, GLN208	TYR211
CHEMBL447424	−1.462	−10.9	VAL94, LEU97, TRP101, LEU117, LEU122, GLN174,TYR211, THR215, TYR283, TYR290, VAL304, PHE308	SER118, TYR283	TRP291
CHEMBL448656	−1.531	−10.6	TRP101, LEU122, TYR211, TYR283, VAL304, PHE308	SER118, THR198, CYS200, GLN208, ASN212, THR215, TRP291	HIS199, PHE308
CHEMBL449373	−0.672	−11.5	VAL94, TRP108, LEU117, LYS121, LEU122, TYR211, TYR283, VAL304, PHE308	SER118, GLN174, CYS200, GLN208, ASN212, TRP291	HIS199, PHE308
CHEMBL450414	−1.544	−10.4	VAL94, TRP101, LEU117, LYS121, TYR211, THR215,TYR290, VAL304, PHE308	GLN208, ASN212,THR215	–
CHEMBL452198	−1.991	−10.4	TRP101, LEU117, THR198, TYR211, THR215, TYR290, PHE308	GLN208, ASN212	TRP291
CHEMBL452474	−1.004	−11.3	VAL94, TRP101, LEU117, LEU122, TYR211, TYR283, VAL304, PHE308	SER118, THR198, CYS200, GLN208, ASN212, TRP291	HIS199, PHE308
CHEMBL455769	−1.505	−10.4	TRP101, LEU117, LEU122, GLN174, THR198, TYR211, TYR283, TYR284, VAL304, PHE308	TYR283	TYR211
CHEMBL456279	−4	−9.9	VAL94,TRP101, LEU117, LYS121, TYR211, THR215, VAL304	CYS200, GLN208, ASN212, THR215	TYR283, PHE308
CHEMBL499442	−2.190	−10.5	VAL94, LEU97, TRP101, LEU117, LYS121, LEU122, TYR211, TYR290, VAL304, PHE308	SER118, GLN208, ASN212, THR215, TRP291	–

Table 3 (continued)

CHEMBL ID	-log (ki)	Dock score (kcal mol^{-1})	Hydrophobic interactions	Hydrogen bonding	pi-pi stacking
CHEMBL499588	−4	−9.7	VAL94, LEU97, ASP98, TRP101, LEU117, LYS121, LEU122, VAL304, PHE308	CYS200, TRP291	–
CHEMBL499849	−3.591	−9.7	TRP101, LEU117, LEU122, PHE170, GLN174, TYR211, VAL304, PHE308	CYS200, GLN208, ASN212, TYR283	TYR211, TRP291
CHEMBL502967	−1.431	−10.6	TRP101, LEU117, LYS121, LEU122, GLN174, THR198, TYR211, TYR290, PHE308	LYS121, GLN208, ASN212	TYR211
CHEMBL505033	−0.080	−11.6	VAL94, TRP101, LEU117, LYS121, HIS199, TYR211, TYR283, TYR284, VAL304, PHE308	GLN208, ASN212, THR215, TRP291	–
CHEMBL506338	−0.969	−10.9	VAL94, LEU97, TRP101, LEU117, LYS121, TYR283, VAL304	SER118, THR198, CYS200, GLN208	HIS199, TYR283, PHE308
CHEMBL508020	−0.556	−11.1	VAL94, LEU97,TRP101, LEU117, LYS121, LEU122, GLN174, TYR211, TYR283, PHE308	CYS200, GLN208, ASN212, TYR283, TRP291	HIS199, TYR283
CHEMBL508435	−0.518	−11.3	VAL94, LEU97, TRP101, LEU117, LEU122, GLN174, TYR211, VAL304, PHE308	THR198, GLN208	TYR283, PHE308
CHEMBL509075	−0.301	−11.6	VAL94, TRP101, LEU117, LEU122, TYR211, TYR283, TYR284, VAL304, PHE308	CYS200, ASN212, THR215, TYR283	TRP291, PHE308
CHEMBL509347	−1.580	−10.6	TRP101, LEU117, LEU122, TYR211, THR215, VAL304, PHE308	GLN208, ASN212, TYR283	TRP291

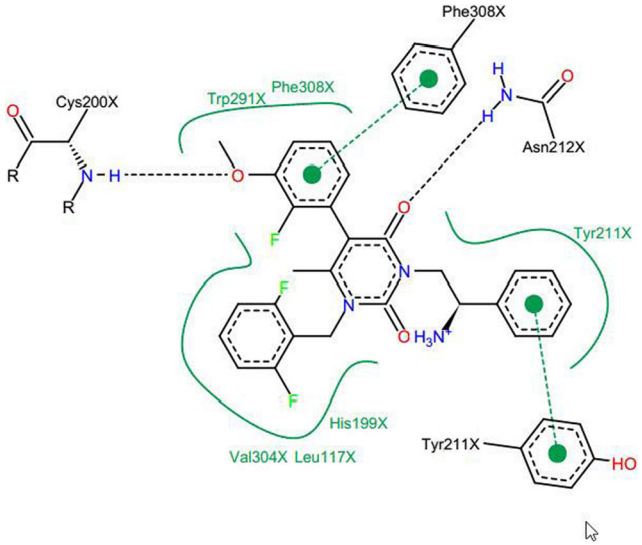

Fig. 6 Binding site interaction of CHMBL179691 by GnRHR receptor

order to ensure that the obtained frame (frame 194) is in accordance with all the structural features reported in the literature, visualization of the structure was done by means of the VMD software. As seen in Fig. 7a, based on orthographic views of the molecule, two conserved disulfide bridges are present in the final structure (CYS14-200 and CYS114-196). At least, one conserved disulfide bridge has been reported for most studies related to GPCRs family [51–54]. Specific recognition of the salt bridges locations is essential for correct folding of the third protein structure [55]. The two specific residues that make the bridge need to be as close as the extent of one water molecule to form an ionic lock. In this study, a known ionic lock is also present between GLU90 and LYS 121. This ionic lock is necessary for correct folding of the receptor within the lipid membrane [22]. In a previuos study, comparative modeling of GnRH receptor based on the structure of rhodopsin and its 35 ns simulation within DPPC membrane has been reported. Frame 194 of the present experiment, describing the receptor at antagonist state, was superposed with the aforementioned model at TM regions. As depicted in Fig. 7b, the two models were similar in TM1 and TM2 regions (RMSD = 1.2 Å and 1.05 Å, respectively). On the other hand relatively higher differences were observed in the case of TM7 and TM6 regions (RMSD = 3.07 Å and 2.51 Å, respectively) [13].

Mobility of the binding site residues was also studied by plotting the RMSD values of the related residues during simulation. As seen in Fig. 8 (left) fluctuations of binding cavity was stabilized during the final steps of simulation with an RMSD average of 2 Å. A more detailed study was done in the case of those frames with more than 0.5 correlation toward experimental activity vector. As seen in Fig. 8 (right), frame 196 was

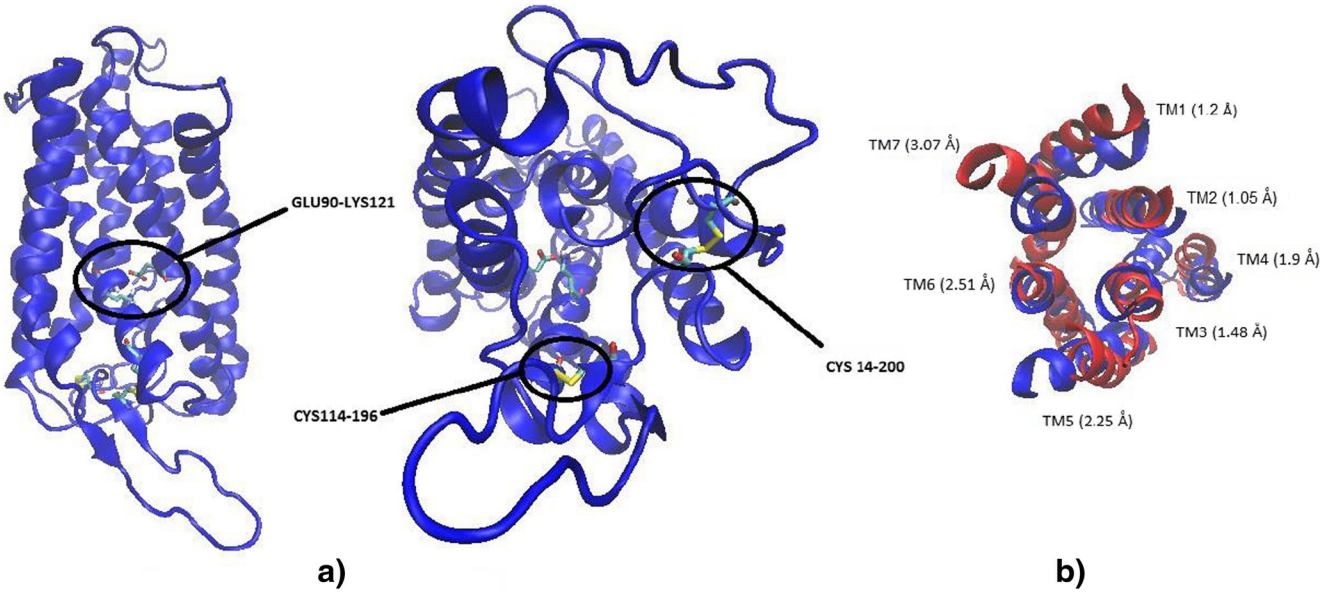

Fig. 7 **a** Orthographic view of frame 194, presence of ionic lock (GLU90-LYS121) and two disulfide bridges (CYS114-200 and CYS114-196) in frame 194 of human GnRH receptor **b** Comparison of the obtained model (frame 194, blue) with another model reported in literature (red)

more similar to frame 194 in terms of the binding cavity residues (RMSD = 0.88 Å). The largest distance was seen in frame 25 representing the receptor at the early stage of simulation (RMSD = 1.88 Å).

Based on the aforementioned experiments and validations, the described model of the receptor can be a promising target for future studies related to drug design for human GnRH receptor. The pdb format of frame 194 is provided in Supplementary information.

Conclusions

A 3D structure for GnRH human receptor at the antagonist state was introduced applying in silico methods. Ramachandran plot confirmed that the threading based model was in accordance with the native proteins. Conserved disulfide bridges were particularly introduced in the model. Different samples of the receptor were extracted based on molecular dynamic simulation and the binding site state was

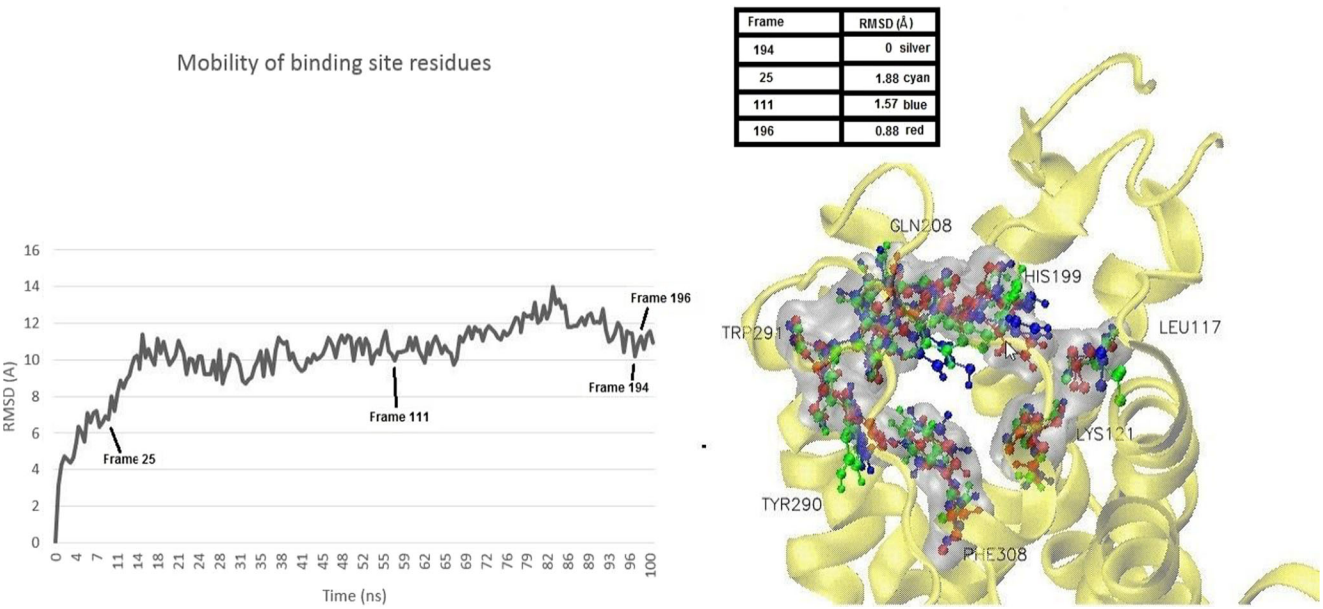

Fig. 8 Mobility of binding site residues during simulation

assessed using a cross docking method of known antagonists. One frame was approved based on Pearson correlation and SSLR studies and verified that our computational method could perfectly emulate the GnRHR at the antagonist state. The presented model would play a pivotal role in the future drug design studies to discover new ligands. The strategy used in this study was sampling different frames of a G-protein coupled receptor at different states of simulation and performing cross-docking simulations on the extracted frames with known inhibitors. This strategy of calibrating computational analysis with experimental data can be used in the case of other membrane receptors to yield reliable models for structure based drug design studies.

Compliance with ethical standards

Conflict of interest All the authors declare that they have no conflict of interest.

Ethical approval This article does not contain any studies with human participants or animals performed by any of the authors.

Informed consent This article does not contain any human participant.

References

1. Ulloa-Aguirre A, Timossi C (2000) Biochemical and functional aspects of gonadotrophin-releasing hormone and gonadotrophins. Reprod BioMed Online 1(2):48–62
2. Speroff L, Fritz MA (2005) Clinical gynecologic endocrinology and infertility. Lippincott Williams & Wilkins, Philadelphia
3. Torrealday S, Lalioti MD, Guzeloglu-Kayisli O, Seli E (2013) Characterization of the gonadotropin releasing hormone receptor (GnRHR) expression and activity in the female mouse ovary. Endocrinology 154(10):3877–3887
4. Sealfon SC, Weinstein H, Millar RP (1997) Molecular mechanisms of ligand interaction with the gonadotropin-releasing hormone receptor. Endocr Rev 18(2):180–205
5. Garner KL, Perrett RM, Voliotis M, Bowsher C, Pope GR, Pham T, Caunt CJ, Tsaneva-Atanasova K, McArdle CA (2015) Information transfer in gonadotropin-releasing hormone (GnRH) signaling: extracellular signal-regulated kinase (ERK)-mediated feedback loops control hormone sensing. J Biol Chem:jbc. M115. 686964
6. López de Maturana R, Pawson AJ, Lu Z-L, Davidson L, Maudsley S, Morgan K, Langdon SP, Millar RP (2008) Gonadotropin-releasing hormone analog structural determinants of selectivity for inhibition of cell growth: support for the concept of ligand-induced selective signaling. Mol Endocrinol 22(7):1711–1722
7. Filicori M (1994) Gonadotrophin-releasing hormone agonists. Drugs 48(1):41–58
8. Kwok C, Treeck O, Buchholz S, Seitz S, Ortmann O, Engel J (2015) Receptors for luteinizing hormone-releasing hormone (GnRH) as therapeutic targets in triple negative breast cancers (TNBC). Target Oncol 10(3):365–373
9. Pawson AJ, Morgan K, Maudsley SR, Millar RP (2003) Type II gonadotrophin-releasing hormone (GnRH-II) in reproductive biology. Reproduction 126(3):271–278
10. Millar RP, Lu Z-L, Pawson AJ, Flanagan CA, Morgan K, Maudsley SR (2004) Gonadotropin-releasing hormone receptors. Endocr Rev 25(2):235–275
11. Lu Z-L, Gallagher R, Sellar R, Coetsee M, Millar RR (2005) Mutations remote from the human gonadotropin-releasing hormone (GnRH) receptor binding sites specifically increase binding affinity for GnRH II, but not GnRH I: evidence for ligand-selective receptor active conformations. J Biol Chem
12. Millar RP, Pawson AJ, Morgan K, Rissman EF, Lu Z-L (2008) Diversity of actions of GnRHs mediated by ligand-induced selective signaling. Front Neuroendocrinol 29(1):17–35
13. Jardón-Valadez E, Ulloa-Aguirre A, An P (2008) Modeling and molecular dynamics simulation of the human gonadotropin-releasing hormone receptor in a lipid bilayer. J Phys Chem B 112(34):10704–10713
14. Kenneth M, Merz J, Ringe D, Reynolds C (2010) Drug design: structure and ligand-based approaches, vol 1. Cambridge University Press, New York, pp 197–257
15. Lanier MC, Feher M, Ashweek NJ, Loweth CJ, Rueter JK, Slee DH, Williams JP, Zhu Y-F, Sullivan SK, Brown MS (2007) Selection, synthesis, and structure–activity relationship of tetrahydropyrido [4, 3-d] pyrimidine-2, 4-diones as human GnRH receptor antagonists. Bioorg Med Chem 15(16):5590–5603
16. Tundidor-Camba A, Caballero J, Coll D (2013) 3D-QSAR modeling of non-peptide antagonists for the human luteinizing hormone-releasing hormone receptor. Med Chem 9(4):560–570
17. Cavasotto CN, Phatak SS (2009) Homology modeling in drug discovery: current trends and applications. Drug Discov Today 14(13): 676–683
18. Schmidt T, Bergner A, Schwede T (2014) Modelling three-dimensional protein structures for applications in drug design. Drug Discov Today 19(7):890–897
19. Katritch V, Rueda M, Lam PCH, Yeager M, Abagyan R (2010) GPCR 3D homology models for ligand screening: lessons learned from blind predictions of adenosine A2a receptor complex. Proteins Struct Funct Bioinformatics 78(1):197–211
20. França TCC (2015) Homology modeling: an important tool for the drug discovery. J Biomol Struct Dyn 33(8):1780–1793
21. Khoddami M, Nadri H, Moradi A, Sakhteman A (2015) Homology modeling, molecular dynamic simulation, and docking based binding site analysis of human dopamine (D4) receptor. J Mol Model 21(2):1–10
22. Conn PM, Ulloa-Aguirre A (2010) Trafficking of G-protein-coupled receptors to the plasma membrane: insights for pharmacoperone drugs. Trends Endocrinol Metab 21(3):190–197
23. Gasteiger E, Gattiker A, Hoogland C, Ivanyi I, Appel RD, Bairoch A (2003) ExPASy: the proteomics server for in-depth protein knowledge and analysis. Nucleic Acids Res 31(13):3784–3788
24. Zhang Y (2008) I-TASSER server for protein 3D structure prediction. BMC Bioinformatics 9(1):40
25. Laskowski RA, MacArthur MW, Moss DS, Thornton JM (1993) PROCHECK: a program to check the stereochemical quality of protein structures. J Appl Crystallogr 26(2):283–291
26. Bernsel A, Viklund H, Hennerdal A, Elofsson A (2009) TOPCONS: consensus prediction of membrane protein topology. Nucleic Acids Res 37(suppl 2):W465–W468
27. Tusnady GE, Simon I (1998) Principles governing amino acid composition of integral membrane proteins: application to topology prediction. J Mol Biol 283(2):489–506
28. Cserzö M, Wallin E, Simon I, von Heijne G, Elofsson A (1997) Prediction of transmembrane alpha-helices in prokaryotic membrane proteins: the dense alignment surface method. Protein Eng 10(6):673–676
29. Hirokawa T, Boon-Chieng S, Mitaku S (1998) SOSUI: classification and secondary structure prediction system for membrane proteins. Bioinformatics 14(4):378–379

30. Sonnhammer EL, Von Heijne G, Krogh A (1998) A hidden Markov model for predicting transmembrane helices in protein sequences. Proc Int Conf Intell Syst Mol Biol 6:175-82
31. Hofman K (1993) TMbase-A database of membrane spanning protein segments. Biol Chem Hoppe-Seyler 374:166
32. Rost B, Yachdav G, Liu J (2004) The predictprotein server. Nucleic Acids Res 32(suppl 2):W321–W326
33. Käll L, Krogh A, Sonnhammer EL (2005) An HMM posterior decoder for sequence feature prediction that includes homology information. Bioinformatics 21(suppl 1):i251–i257
34. Shokri A, Abedin A, Fattahi A, Kass SR (2012) Effect of hydrogen bonds on p K a values: importance of networking. J Am Chem Soc 134(25):10646–10650
35. Pronk S, Páll S, Schulz R, Larsson P, Bjelkmar P, Apostolov R, Shirts MR, Smith JC, Kasson PM, van der Spoel D (2013) GROMACS 4.5: a high-throughput and highly parallel open source molecular simulation toolkit. Bioinformatics 29(7):845–854
36. Humphrey W, Dalke A, Schulten K (1996) VMD: visual molecular dynamics. J Mol Graph 14(1):33–38
37. Schmidt TH, Kandt C (2012) LAMBADA and InflateGRO2: efficient membrane alignment and insertion of membrane proteins for molecular dynamics simulations. J Chem Inf Model 52(10):2657–2669
38. Kandt C, Ash WL, Tieleman DP (2007) Setting up and running molecular dynamics simulations of membrane proteins. Methods 41(4):475–488
39. Allen WJ, Lemkul JA, Bevan DR (2009) GridMAT-MD: a grid-based membrane analysis tool for use with molecular dynamics. J Comput Chem 30(12):1952–1958
40. Morris GM, Huey R, Olson AJ (2008) Using autodock for ligand-receptor docking. Curr Protocol Bioinformatics doi: 10.1002/0471250953.bi0814s24
41. Gaulton A, Bellis LJ, Bento AP, Chambers J, Davies M, Hersey A, Light Y, McGlinchey S, Michalovich D, Al-Lazikani B (2012) ChEMBL: a large-scale bioactivity database for drug discovery. Nucleic Acids Res 40(D1):D1100–D1107
42. Källberg M, Wang H, Wang S, Peng J, Wang Z, Lu H, Xu J (2012) Template-based protein structure modeling using the RaptorX web server. Nat Protoc 7(8):1511–1522
43. Dundas J, Ouyang Z, Tseng J, Binkowski A, Turpaz Y, Liang J (2006) CASTp: computed atlas of surface topography of proteins with structural and topographical mapping of functionally annotated residues. Nucleic Acids Res 34(suppl 2):W116–W118
44. Trott O, Olson AJ (2010) AutoDock Vina: improving the speed and accuracy of docking with a new scoring function, efficient optimization, and multithreading. J Comput Chem 31(2):455–461
45. Hevener KE, Zhao W, Ball DM, Babaoglu K, Qi J, White SW, Lee RE (2009) Validation of molecular docking programs for virtual screening against dihydropteroate synthase. J Chem Inf Model 49(2):444–460
46. Baugh EH, Lyskov S, Weitzner BD, Gray JJ (2011) Real-time PyMOL visualization for Rosetta and PyRosetta. PLoS One 6(8):e21931
47. Salentin S, Schreiber S, Haupt VJ, Adasme MF, Schroeder M (2015) PLIP: fully automated protein–ligand interaction profiler. Nucleic Acids Res 43(W1):W443–W447
48. Källberg M, Margaryan G, Wang S, Ma J, Xu J (2014) RaptorX server: a resource for template-based protein structure modeling. Protein Struct Prediction:17–27
49. Lu Z-L, Coetsee M, White CD, Millar RP (2007) Structural determinants for ligand-receptor conformational selection in a peptide G protein-coupled receptor. J Biol Chem 282(24):17921–17929
50. Engel J (2012) Use of LHRH antagonists for intermittent treatments. Patent US 8273716 B2
51. Sakhteman A, Lahtela-Kakkonen M, Poso A (2011) Studying the catechol binding cavity in comparative models of human dopamine D 2 receptor. J Mol Graph Model 29(5):685–692
52. Wu B, Chien EY, Mol CD, Fenalti G, Liu W, Katritch V, Abagyan R, Brooun A, Wells P, Bi FC (2010) Structures of the CXCR4 chemokine GPCR with small-molecule and cyclic peptide antagonists. Science 330(6007):1066–1071
53. Palczewski K, Kumasaka T, Hori T, Behnke CA, Motoshima H, Fox BA, Le Trong I, Teller DC, Okada T, Stenkamp RE (2000) Crystal structure of rhodopsin: AG protein-coupled receptor. Science 289(5480):739–745
54. Zhang K, Zhang J, Gao Z-G, Zhang D, Zhu L, Han GW, Moss SM, Paoletta S, Kiselev E, Lu W (2014) Structure of the human P2Y12 receptor in complex with an antithrombotic drug. Nature 509(7498):115
55. Cook JV, Eidne KA (1997) An intramolecular disulfide bond between conserved extracellular cysteines in the gonadotropin-releasing hormone receptor is essential for binding and activation 1. Endocrinology 138(7):2800–2806